Effect of magnesium ferrite doping with lanthanide ions on dark-, visible- and UV-driven Methylene Blue degradation on heterogeneous Fenton-like catalysts

Andrei Ivanets[1*], Vladimir Prozorovich[1], Valentin Sarkisov[1], Marina Roshchina[1], Inga Grigoraviciute-Puroniene[2], Aleksej Zarkov[2], Aivaras Kareiva[2], Vhahangwele Masindi[3], Chongqing Wang[4], Varsha Srivastava[5, 6], Mika Sillanpää[7-12]

[1]Institute of General and Inorganic Chemistry of National Academy of Sciences of Belarus, st. Surganova 9/1, 220072 Minsk, Belarus, ivanets@igic.bas-net.by

[2]Institute of Chemistry, Vilnius University, Naugarduko 24, LT-03225 Vilnius, Lithuania

[3]Department of Environmental Sciences, College of Agriculture and Environmental Sciences, University of South Africa, P.O. Box 392, Florida, 1710, South Africa

[4]School of Chemical Engineering, Zhengzhou University, Zhengzhou 450001, China

[5]Department of Green Chemistry, LUT University, Sammonkatu 12, FI-50130 Mikkeli, Finland

[6] Research Unit of Sustainable Chemistry, Faculty of Technology, University of Oulu, Oulu 90014, Finland

[7]Department of Chemical Engineering, School of Mining, Metallurgy and Chemical Engineering, University of Johannesburg, P. O. Box 17011, Doornfontein 2028, South Africa

[8]Chemistry Department, College of Science, King Saud University, Riyadh 11451, Saudi Arabia

[9]School of Resources and Environment, University of Electronic Science and Technology of China (UESTC),

NO. 2006, Xiyuan Ave., West High-Tech Zone, Chengdu, Sichuan 611731, P.R. China

[10]Faculty of Science and Technology, School of Applied Physics, University Kebangsaan Malaysia, 43600, Bangi, Selangor, Malaysia

[11]School of Chemistry, Shoolini University, Solan, Himachal Pradesh, 173229, India

[12]Department of Biological and Chemical Engineering, Aarhus University, Nørrebrogade 44, 8000 Aarhus C, Denmark

Abstract. The catalytic behavior of magnesium ferrites doped with lanthanide ions (La^{3+}, Ce^{3+}, Sm^{3+}, Gd^{3+}, and Dy^{3+}) on Methylene Blue (MB) degradation using Fenton process was studied. A slow increase in cubic *Fd3m* crystalline structure parameters (lattice parameter *a* of 8.362 – 8.400 Å, cell volume *V* of 0.5848 – 0.5999 nm^3) and increase in crystallite size (*D* of 11.30 – 15.45 nm) of doped samples magnesium ferrites were observed. A dramatic decrease in catalytic activity of catalysts obtained at 600 °C as compared to catalysts obtained at 300 °C was explicitly observed and this was grossly attributed to the elimination of surface hydroxyl groups as ascertained by FT-IR analysis. The initial magnesium ferrite demonstrated the highest catalytic activity under dark- (k' 0.0555 min^{-1}) and visible-light (k' 0.1029 min^{-1}) conditions. Catalytic efficiency of the lanthanides doped catalysts under UV-irradiation in accordance with the maximum appearance rate constant k' decreased in the following order $Ce^{3+} > Dy^{3+} > La^{3+} \approx MgFe_2O_4 > Sm^{3+} > Gd^{3+}$. The most active ferrites provided up to 99 % of MB degradation in 60 and 20 min for visible- and UV-driven Fenton processes. Findings obtained from this study were observed to be competitive with other heterogeneous Fenton catalysts.

Keywords: Magnesium ferrite; Lanthanide ions doping; Heterogeneous Fenton-like catalysts; Methylene Blue degradation; Mechanism catalytic.

1 Introduction

Ferrite-spinels, due to their unique structural, chemical, and magnetic properties, are used for biomedical, adsorption, and catalytic applications [1-8]. Depending on the crystalline structure and distribution of cations of divalent and trivalent metals in tetrahedral and octahedral positions, ferrite-spinels are divided into normal and reversed [9, 10]. Ideally, normal spinels with the general formula AB_2O_4 consist of divalent A cations occupying 1/8 of the tetrahedral positions, and trivalent B cations occupying 1/2 of the octahedral positions. However, in the case of reversed spinel, the general formula can be represented as $B(AB)O_4$, where the tetrahedral positions are occupied by trivalent B cations, while the divalent A

cations and trivalent B cations are evenly distributed in the octahedral positions. Thus, part of the voids remains unfilled, which makes it possible for the redistribution of metal ions between the voids. The intermediate state between normal and reversed spinel leads to the formation of mixed spinel, which is typical for several metal ferrites. At the same time, the properties of intermediate spinels are greatly influenced by the nature and ratio of cations located in tetrahedral and octahedral positions [11-13].

Magnesium ferrite ($MgFe_2O_4$) belongs to the mixed spinel-type (degree of inversion ~ 0.9), is a soft ferromagnet and an n-type semiconductor with a cubic crystal lattice belonging to the space group *Fd3m* [14]. The possibility of placing various cations, whose ionic radius is in the range of 0.6 – 0.9 Å, in octahedral and tetrahedral positions allows us to directionally vary the properties of metal ferrites. This is important for controlling the physicochemical properties of magnesium ferrite, which improves their functional characteristics, including magnetic, adsorption, and catalytic properties [15-17].

Doping ferrites with even a small amount of lanthanides lead to significant structural distortions and deformation of their lattice, which causes changes in the physicochemical and, accordingly, functional properties. Due to the larger radius of lanthanide ions, as a rule, substitution occurs only in octahedral voids, which leads to an increase in the crystal lattice parameter [18-20]. The substitution of metal ions for lanthanide ions in the ferrite crystal lattice can lead to an increase in the efficiency of the catalytic destruction of organic molecules in several ways. Thus, in the case of a Fenton-like reaction, the introduction of lanthanide into the ferrite matrix can lead to an improvement in the reversibility of the Fe^{3+}/Fe^{2+} redox pair, which is responsible for the generation of HO· radicals due to the interaction of 3d-4f orbitals. In the case of the photo-Fenton reaction, the introduction of lanthanide ions can improve the absorption of visible light by forming impurity states in the band gap due to the lower electron transition energy from the valence band to the 4f-orbitals of the lanthanide ion. In addition, some lanthanide ions can form their redox pairs, for example, Ce^{4+}/Ce^{3+}, and thus activate Fenton-like processes in parallel with the participation

of the Fe^{3+}/Fe^{2+} pair [21]. The authors [19] showed that the doping of magnesium ferrite with Nd^{3+}, Sm^{3+}, and Dy^{3+} ions leads to structural distortions and significantly changes its electrical, magnetic, and catalytic properties in the decomposition reaction of 4-chlorophenol. Magnesium ferrite is an environmentally friendly and non-toxic magnetic material, which makes it suitable for water purification [3]. Previously the effect of the adsorption of transition metal ions (Mn^{2+}, Co^{2+}, Ni^{2+}, Cu^{2+}) on the catalytic activity of magnesium ferrite was established, which was chosen as a Fenton-like catalyst. The possibility of the participation of transition metal cations with variable valence as initiators of the formation of HO· radicals, as the main reactive oxygen-containing particles formed during the catalytic destruction of hydrogen peroxide, was shown [22]. An important result was the establishment of the relationship between the nature of the adsorbed cation and the degree of its desorption on the catalytic activity of modified magnesium ferrite. The stability of the crystal structure and texture characteristics of magnesium ferrite in the processes of adsorption and catalysis has been proved by X-ray diffraction, IR spectroscopy, and low-temperature nitrogen adsorption-desorption [23]. Despite a significantly large number of publications devoted to the preparation of adsorbents and catalysts based on metal ferrites, including studies of the effect of metal ions doping, data on the preparation of Fenton-like catalysts based on magnesium ferrite doped with lanthanide ions have not been found.

This study aims to develop heterogeneous Fenton catalysts based on lanthanide-doped (La^{3+}, Ce^{3+}, Sm^{3+}, Gd^{3+}, and Dy^{3+}) magnesium ferrite. The following important tasks were investigated: (i) the influence of lanthanide ions on the crystal structure parameters of magnesium ferrite was established; (ii) the role of the calcination temperature of magnesium ferrite and the reasons for the decrease in their catalytic activity were revealed; and (iii) the possibility of controlling the efficiency of methylene blue degradation in dark-, visible- and UV-driven Fenton processes was demonstrated.

2 Materials and Methods

2.1 Catalysts preparation

$Mg(NO_3)_2$, $Fe(NO_3)_3$, $La(NO_3)_3$, $Ce(NO_3)_3$, $Sm(NO_3)_3$, $Gd(NO_3)_3$, $Dy(NO_3)_3$, NaCl, and glycine (amino acetic acid, H_2NCH_2COOH) reagents were obtained from Five Ocean Company, Ltd, Belarus and they were used for the synthesis of magnesium ferrites without any additional purification. Magnesium ferrites doping with La^{3+}, Ce^{3+}, Sm^{3+}, Gd^{3+}, and Dy^{3+} were prepared by a modified glycine-nitrate method [24] with the addition of a 10.0 mol. % lanthanide nitrate salt to the reaction mixture relative to iron ions. Glycine (H_2NCH_2COOH) was introduced into the reaction mixture as a complexing additive and fuel for self-propagating in high-temperature synthesis. To prevent the aggregation of highly dispersed magnesium ferrite particles, the addition of sodium chloride NaCl was used, which forms an inert shell on the surface of the resulting oxide nanoparticles. The reaction mixture was pre-evaporated under constant intensive stirring until a viscous dark brown gel was formed, which was then heated in a SNOL 1.7/1300 furnace at a speed of 5 °/ min with exposure at 300 and 600 °C for 5 h. Magnesium ferrite nanoparticles were separated by magnetic separation thenceforth, the obtained black powder was washed using distilled water to remove impurities. For quality control, ultra-pure water (18.2 MΩ·cm) was used for all the experiments.

2.2 Physical-chemical methods

X-ray diffraction (XRD) of the obtained magnesium ferrite samples was performed using an Empyrean X-ray diffractometer (PANalytical, the Netherlands) with Co-$K_{\alpha 1}$ radiation (λ 0.1789 nm) in the range 2Θ of 20-80 °. To determine the phase composition of the samples under study, the programs "PowderX" and "WinXpow" were used, as well as the database of radiographic powder standards "JCPDS PDF2". The crystallite sizes were analyzed using the "Size / Strain" program of the "WinXpow" software package according to the Scherrer equation:

$$d = 0.9 \times \lambda / \beta \times \cos\theta, \quad (1)$$

where d is the average size of the crystallites, nm; λ is the wavelength of the X-ray radiation, nm; β is the width of the half-height reflex, rad; θ is the Bragg angle, deg.

IR spectra of doped magnesium ferrite samples were recorded on an IR Affinity-1 Fourier transform spectrometer (Shimazu, Japan) in the range of ν 400-4000 cm^{-1}. Previously, the samples were crushed in an agate mortar and pressed into tablets with KBr. The morphology and elemental composition of magnesium ferrites were studied using a scanning electron microscope (SEM) JSM-5610 LV (JEOL, Japan) with an energy-dispersive X-ray (EDX) prefix JED-2201 (JEOL, Japan) and a transmission electron microscope (TEM) 7700 (Hitachi, Japan).

2.3 Catalytic Methylene Blue degradation

To exclude the influence of competing adsorption process, the catalysts were saturated with the Methylene Blue solution (100 mg/L) in the dark for 30 min. Furthermore, 25.0 mg of catalyst and 100 μL of 30 wt. % H_2O_2 solution (20 mmol/L) were added to the 50.0 mL dye aliquot (10.0 mg/mL; pH 8.0; 20 °C). To evaluate the kinetic dependences, samples were taken after 5; 10; 20; 30; 40, and 60 min. The catalytic experiment was carried out using a diode (λ = 650 – 670 nm) and UV-C lamps (λ = 200 – 280 nm) as a source of visible- and UV-radiation, respectively.

In all experiments, model solutions were mixed at a speed of 300 rpm by the rotary shaker ST15 (Cat, M. Zipperer GmbH, Staufen, Germany). The pH of initial solutions was estimated by pH meter of 340i (±0.02) (Mettler Toledo, USA). The temperature of the model solutions was 20 °C. The dye concentration was measured using the scanning spectrophotometer SP-8001 (Metertech, Taiwan) at the most intense absorption wavelength of 664 nm. The degree of MB mineralization/degradation was determined via a Total Organic Carbon Analyzer TOC-V CPH/CPN (Shimadzu, Japan). All the catalytic experiments were performed in double tests and reported as mean values. The error of the experiment was deemed valid if the final value did not exceed 3 %.

The degree (α, %) of the catalytic degradation of Methylene Blue was calculated by the equation:

$$\alpha = (1 - C_0/C_t) \times 100 , \quad (2)$$

Where, C_0 and C_t are the initial and equilibrium Methylene Blue concentrations, mg/L; t is the time, min.

The values of apparent velocity constant (k', min^{-1}) were determined graphically from the first-order reaction equation:

$$\ln(C_0/C_t) = k' \times t \quad (3)$$

3 Results and Discussion

3.1 XRD and FT-IR

Fig. 1 shows X-ray patterns of magnesium ferrite samples obtained at 300 and 600 °C. According to the data of X-ray phase analysis, the sample obtained without the introduction of dopant ions at 300 °C denotes a weakly-crystallized magnesium ferrite with low-intensity reflexes corresponding to the planes (220), (311), (400), (511), (404) (Fig. 1a). An increase in the calcination temperature to 600 °C led to a noticeable increase in the intensity of these reflexes, which indicates the process of magnesium ferrite crystallization (Fig. 1b).

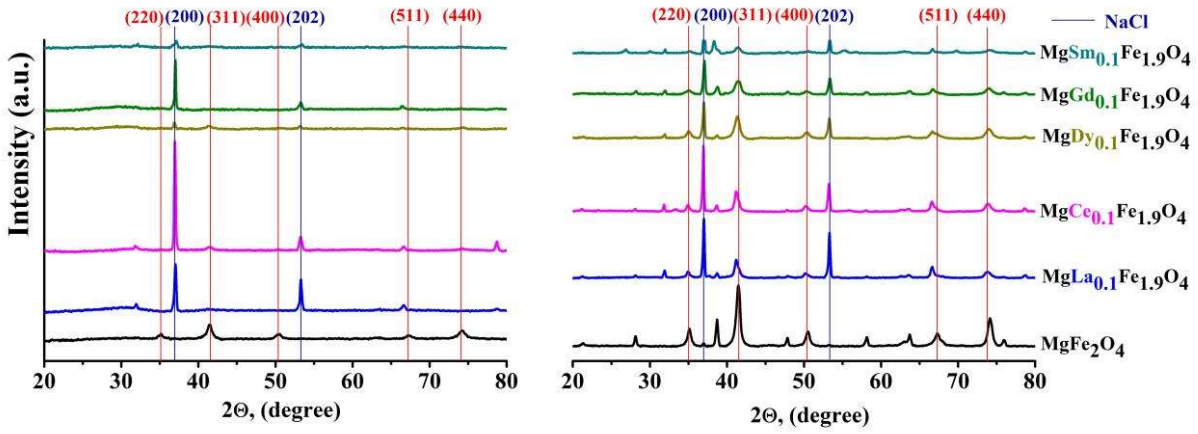

a b

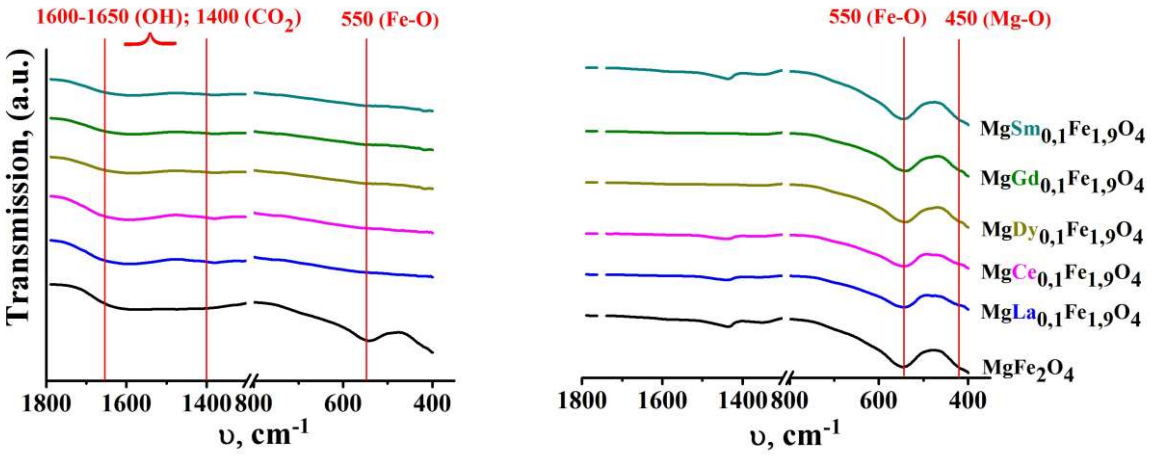

c d

Fig. 1. (a, b) XRD patterns and (c, d) FT-IR spectra of magnesium ferrite samples doped with lanthanides calcined at (a, c) 300 and (b, d) 600 °C.

Doping with lanthanide ions led to a noticeable amorphization of magnesium ferrite, which is confirmed by the absence of magnesium ferrite reflexes on the diffractograms of samples obtained at 300 °C (Fig. 1a). Minor sodium chloride reflexes were present on radiographs, which is due to incomplete washing of the obtained samples. Heat treatment of doped samples at 600 °C was accompanied by the crystallization of magnesium ferrite and the appearance of reflexes characteristic of cubic magnesium ferrite-spinel (Fig. 1b). It is important to note that all synthesized samples were single-phase products and did not contain impurities of iron oxides, orthoferrites, or lanthanide oxides. This confirms the formation of doped magnesium ferrites. The established regularities are in good agreement with the results obtained in the study of the effect of lanthanide ions on the crystal structure and magnetic properties of cobalt ferrite [18].

To confirm the formations of the ferrite-spinel phase, the IR spectra of the obtained samples were analyzed (Figs. 1c, 1d). The IR spectra of the samples obtained at 300 °C show wide bands in the region of 1600 – 1650 cm^{-1}, characteristic of deformation vibrations of OH-groups in adsorbed water molecules, as well as insignificant absorption bands at 1400 cm^{-1}, which may be due to the presence of adsorbed carbon dioxide molecules. The presence of low-intensity absorption bands in the range of 600 to 550 cm^{-1} was due to the valence vibrations of the Fe^{3+}–O^{2-} bond located in tetrahedral positions (Fig. 1c). The IR spectra of

magnesium ferrite samples obtained at 600 °C underwent noticeable changes (Fig. 1d). The absorption bands at 1600-1650 cm^{-1} were almost completely absent, which indicates the processes of dehydration and dehydroxylation of magnesium ferrite. The intensity of the band increased significantly in the region of 550 cm^{-1}, and an absorption band appeared at lower wavenumbers of 385, 450 cm^{-1}, which can be attributed to vibrations of the Mg^{2+}–O^{2-} and Fe^{3+}–O^{2-} bonds located at the nodes of the octahedral lattice. Both absorption bands indicated the formation of magnesium ferrite with a spinel structure.

The influence of the nature of dopant cations on the parameters of the crystal structure of magnesium ferrites obtained at 600 °C was estimated based on the analysis of the calculated values of the crystal lattice parameter *a* (Fig. 2a), the unit cell volume *V* (Fig. 2b), and the average crystallites size *D* (Fig. 2c). The crystallite size, volume, and unit cell parameters for magnesium ferrite samples calcined at 300 °C were difficult to calculate due to the low intensity of X-ray patterns.

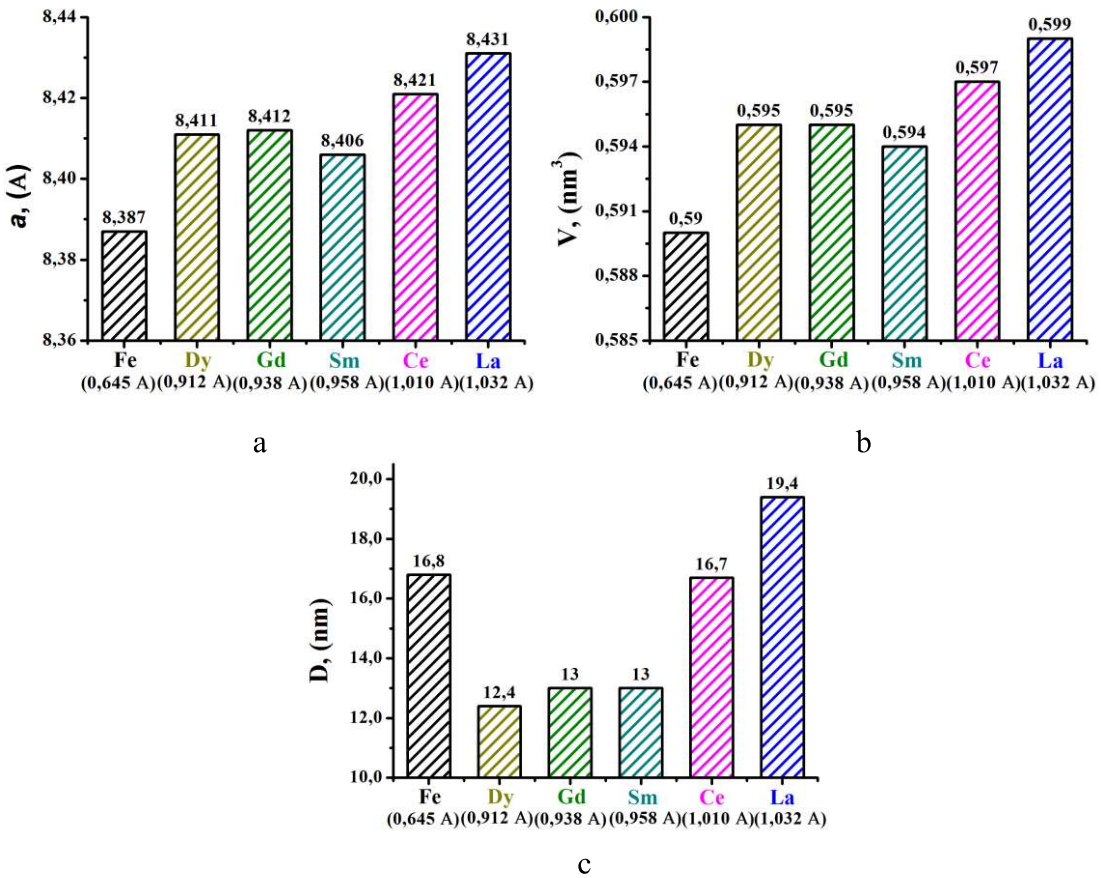

Fig. 2. The changes of (a) the crystal lattice parameter *a*, (b) the unit cell volume *V*, and (c) the average crystallites size *D* of magnesium ferrite samples doped with lanthanides.

Similar patterns were observed for changes in the volume of the unit cell V (Fig. 2b). At the same time, the change in the volume of the unit cell had a less pronounced dependence on the ionic radius of the lanthanide, which was confirmed by a slight change in this parameter for all doped samples, which was in the narrow range of 0.594 – 0.599 nm^3. It should be noted that the introduction of lanthanide ions into the structure of magnesium ferrite resulted in a slight decrease in the size of the crystallites from 16.8 to 12.4 nm for magnesium ferrite and Dy-doped sample, respectively. This indicates the inhibitory effect of lanthanide cations on the growth of magnesium ferrite-spinel crystallites. The exception to this series was the La-doped sample, whose crystallite size was 19.4 nm. At the same time, there was no strict relationship between the ionic radius of the dopant and the average size of the crystallites (Fig. 2c).

3.2 SEM-EDX and TEM

According to the SEM data, all samples of magnesium ferrites were represented by highly dispersed particles formed as a result of the release of a large volume of gaseous combustion products of the glycine-nitrate mixture, which transformed into a sponge-like structure with many large pores of 5-10 μm at 600 °C. Typical SEM images of the surface of La-doped magnesium ferrites sample calcined at 300 and 600 °C are shown in Fig. 3a and Fig. 3c. At the same time, the TEM data are in good agreement with the presented results of the crystallite sizes calculated from the XRD data. Thus, the size of the crystallites identified in the TEM images of magnesium ferrites obtained at 300 (Fig. 3b) and 600 °C (Fig. 3d) was ~2-5 and ~10-15 nm, respectively.

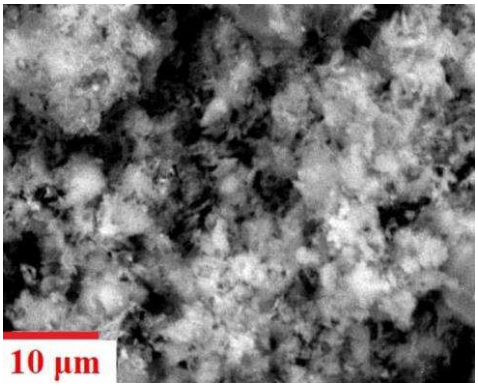

a

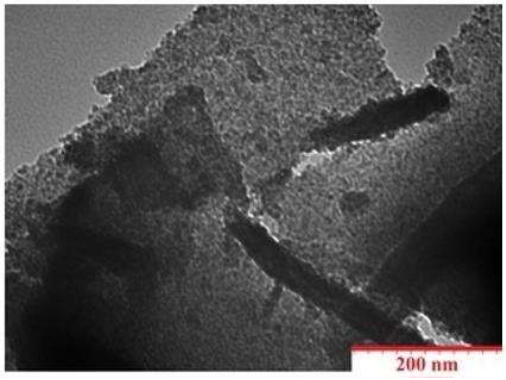

b

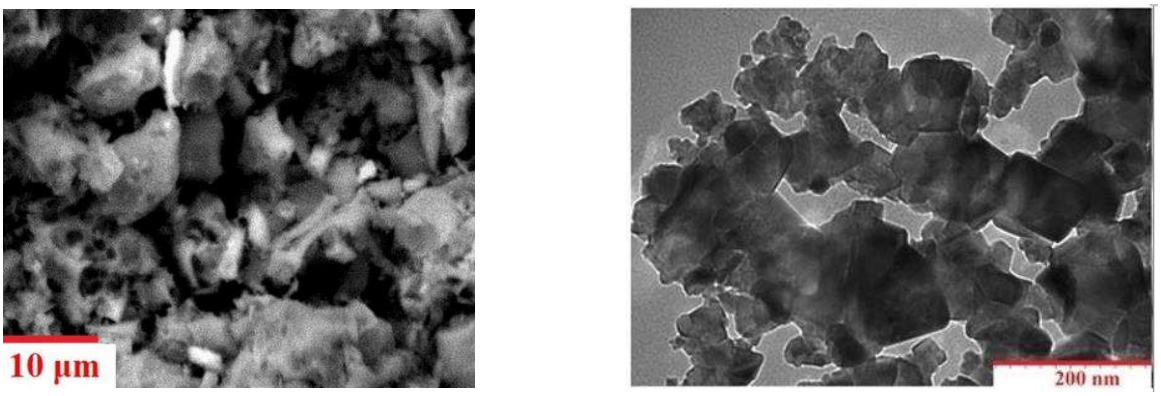

c d

Fig. 3. (a, c) SEM (× 1000) and (b, d) TEM (× 50 000) images of La-doped magnesium ferrites calcined at (a, b) 300 and (c, d) 600 °C.

EDX analysis data (S.1) confirm the introduction of lanthanide ions into the magnesium ferrite composition. At the same time, the ratio of the Mg:Fe:La ion content did not correspond to the stoichiometric value of 1 : 1.9 : 0.1, although the results of the XRD analysis confirm the formation of a single-phase product – cubic spinel of magnesium ferrite. Thus, the lower content of magnesium and lanthanum ions may be due to the concentration on the surface of magnesium ferrite mainly of iron atoms occupying tetrahedral positions. This is in good agreement with the earlier conclusion about the location of Fe^{3+} ions in the octahedral positions occupied by Mg^{2+} ions. An increase in the calcination temperature from 300 to 600 °C led to a decrease in the content of magnesium ions and an increase in the concentration of lanthanum. This was due to the crystallization of doped magnesium ferrite, accompanied by the processes of rearrangement of the crystal structure.

3.3 Dark-, visible- and UV-driven Methylene Blue degradation

Preliminary studies have shown that an increase in the calcination temperature of samples to 600 °C led to a sharp decrease in the catalytic activity of magnesium ferrites (the degree of MB degradation of ~ 10-15 % within 60 min). This result is in good agreement with the IR spectroscopy data (Figs. 1c, 1d) and the previously revealed determining role of surface OH-groups and crystallite sizes on the adsorption properties of magnesium ferrite [22], as the primary stage of the MB catalytic oxidation. In this connection, samples of heterogeneous

Fenton catalysts obtained at 300 °C were of interest for further study of the catalytic activity. The kinetics of the MB degradation under different types of radiation is shown in Figs. 4a, 4c, and 4e.

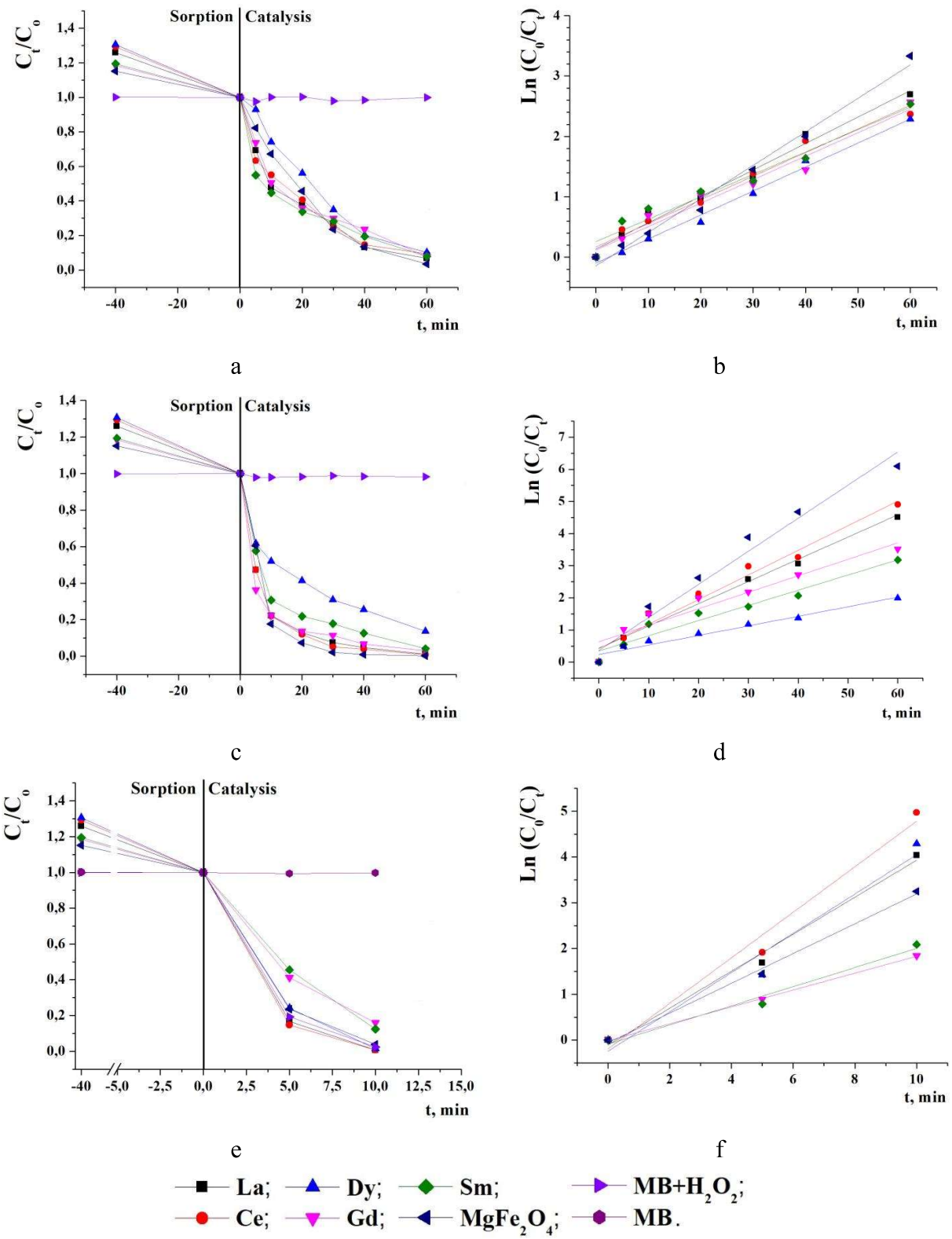

Fig. 4. MB degradation on magnesium ferrites doped with lanthanide ions under (a, b) dark-, (c, d) visible-, (e, f) UV-driven heterogeneous Fenton processes.

The analysis of the obtained data depicts that the interaction of hydrogen peroxide in light did not lead to noticeable dye degradation. Regardless of the dopant ion nature, the degree of MB degradation under visible light reached 95 – 100 % within 60 min. In the case of using UV-radiation, a similar degree of dye degradation was achieved after 20 min. It should be noted that in the latter case, the decomposition of MB in the presence of hydrogen peroxide was also observed without a catalyst as a result of the photolysis of hydrogen peroxide with the generation of ·OH radicals under the influence of UV radiation.

It is known that the photocatalytic degradation of organic dyes is most accurately described by the first-order reaction equation and obeys the Langmuir-Hinschelwood kinetics [25]. This fact was in good agreement with the results of kinetic modeling (Figs. 4b, 4d, and 4f). It was established that the kinetics of the catalytic destruction of the dye with a high degree of confidence ($R^2 \sim 0.96 – 0.99$) was well described by the first-order reaction model.

A comparison of the calculated values of the apparent rate constant of the MB degradation in the presence of magnesium ferrites doped with lanthanides is presented in Table 1.

Table 1. Calculated parameters of first-order kinetic model for MB degradation.

Sample	Initial $MgFe_2O_4$	La	Ce	Dy	Gd	Sm
Dark conditions						
k', min^{-1}	0.0555	0.0438	0.0391	0.0397	0.0389	0.0371
R^2	0.9893	0.9838	0.9762	0.9915	0.9685	0.9608
Visible light						
k', min^{-1}	0.1029	0.0692	0.0765	0.0298	0.0513	0.0472
R^2	0.9715	0.9690	0.9725	0.9647	0.9124	0.9479
UV light						
k', min^{-1}	0.3251	0.4039	0.4972	0.4290	0.1842	0.2089
R^2	0.9960	0.9912	0.9828	0.9636	0.9996	0.9801

When illuminated by their visible radiation spectrum, the calculated values of the apparent rate constant k' were (2.9 – 9.6) $\times 10^{-2}$ min^{-1}, which is ~ 1.3 – 4.3 times lower than that for the initial sample of magnesium ferrite (k' 12.9$\times 10^{-2}$ min^{-1}). In the case of UV irradiation, there was a significant increase in the value of the apparent velocity constant for all samples. At the same time, a more significant increase (~ 1.5 – 17.1 times) was observed for doped magnesium ferrites compared to the initial magnesium ferrite (~ 1.2 times). The results obtained are in good agreement with the data described in a previous study [18].

According to Table 1, magnesium ferrite samples doped with La^{3+}, Ce^{3+}, and Dy^{3+} ions had higher catalytic activity compared to a catalyst based on the initial magnesium ferrite. At the same time, samples doped with Sm^{3+} and Gd^{3+} ions exhibit the least catalytic activity under these conditions. The obtained data on the behavior of the synthesized catalysts are due to different mechanisms of the Fenton and photo-Fenton processes. Thus, the generation of ·OH radicals in the Fenton reaction can be carried out by a single-electron transfer in the interaction of Fe^{2+} ions with hydrogen peroxide (Haber-Weiss mechanism), or by a two-electron mechanism through the transfer of oxygen atoms to form FeO^{2+} (Bray-Gorin mechanism) [26]. At the same time, the introduction of lanthanides into the magnesium ferrite matrix could lead to an increase in their catalytic activity in the photo-Fenton reaction due to the interaction of *3d-4f*-orbitals and increased generation of ·OH radicals, as well as due to the formation of impurity states in the band gap and a decrease in the electron transition energy. The scheme of proposed mechanism of dark-, visible- and UV-driven MB degradation on magnesium ferrite doping with lanthanide ions is shown on S.2.

In addition, it is necessary to take into account the possibility of changing the degree of oxidation of lanthanides under the influence of UV radiation with the formation of redox pairs, which leads to the activation of the photo-Fenton process [18, 27]. Thus, the change in the apparent rate constant of the Methylene Blue oxidation reaction, depending on the nature of the lanthanide ion, was complex.

3.4 Reusability and comparison of catalytic activity

In practice, the most interesting catalysts are those that demonstrate high efficiency of organic pollutants degradation under visible radiation. The possibility of reuse of catalysts is also often a limiting factor in the practical use of the developed Fenton catalysts in wastewater treatment. To determine the stability of the catalytic properties and the possibility of repeated use of synthesized magnesium ferrites, catalytic tests were performed on the example of a La-doped sample under the influence of visible light (Fig. 5). Thus, during four catalytic cycles, a slight decrease in the catalytic activity was observed, which indicated the stability of the structure and the possibility of repeated use of the obtained heterogeneous Fenton catalysts.

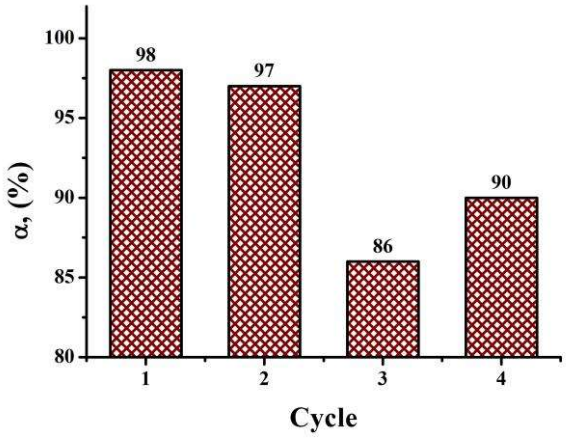

Fig. 5. The catalytic activity of La-doped magnesium ferrite during multiply tests.

The k′ values for the obtained samples exceeded similar characteristics for heterogeneous Fenton catalysts based on ferrites ($Ba_{0.75}Cu_{0.25}Fe_{12}O_{19}$, $rGO/MnFe_2O_4$), as well as nonmetallic ($g\text{-}C_3N_4\text{-}N$) and zero-valence metallic composite (FeNi/C-300) (Table 2). This is also confirmed by a longer time (up to 120 min), which is necessary to achieve comparable values of the MB degradation degree (up to 99 %). For several heterogeneous (Fe_2GeS_4) and homogeneous (MgO_2/Fe^{3+}) Fenton catalysts, the values of the rate constants are not reported. At the same time, the degree of degradation of the dye of more than 99 % was achieved within 10 and 30 min, which is much faster than for La-doped magnesium ferrite.

Table 2. Efficiency of MB degradation with Fenton-like catalyst under visible light irradiation.

Catalyst	Catalytic experiment conditions	Degradation / mineralization, %	k', min^{-1}	Reference
$Ba_{0.75}Cu_{0.25}Fe_{12}O_{19}$	Dose – 0.5 g L^{-1}; C(MB) – 20 mg L^{-1}; C(H_2O_2) – 16.0 mM; pH – 7.0; T – 25°C; t – 120 min.	99.0 / 88.2	0.0434	[28]
g-C_3N_4-N	Dose – 1.0 g L^{-1}; C(MB) – 20 mg L^{-1}; C(H_2O_2) – 199.4 mM; pH – 7.2; T – 25 °C; t – 90 min.	99.0 / -	0.0508	[29]
Fe_2GeS_4	Dose – 0.3 g L^{-1}; C(MB) – 20 mg L^{-1}; C(H_2O_2) – 50.0 mM; pH – 7.0; T – 25 °C; t – 10 min.	99.8 / 56.3	-	[30]
MgO_2/Fe^{3+}	Dose – 0.05 g L^{-1}; C(MB) – 20 mg L^{-1}; C(H_2O_2) – 2.4 M; pH – 6.0; t – 30 min.	99.1 / 70.2	-	[31]
$CuCr_2O_4/CeO_2$	Dose – 0.8 g L^{-1}; C(MB) – 10 mg L^{-1}; C(H_2O_2) – 4.0 mM; pH – 7.0; t – 20 min.	98.0 / -	0.1878	[32]
FeNi/C-300	Dose – 1.0 g L^{-1}; C(MB) – 30 mg L^{-1}; C(H_2O_2) – 20.0 mM; pH – 6.5; T – 25°C; t – 60 min.	99.2 / 59.2	0.0106	[33]
rGO/$MnFe_2O_4$	Dose – 0.25 g L^{-1}; C(MB) – 20 mg L^{-1}; C(H_2O_2) – 120.0 mM; t – 60 min.	80.0 / -	0.0144	[34]
Ln-doped $MgFe_2O_4$	Dose – 0.5 g L^{-1}; C(MB) – 10 mg L^{-1}; C(H_2O_2) – 20.0 mM; pH – 6.0; T – 25°C; t – 60 min.	98.9 / 97.0	0.0692	This work

The most important parameter when choosing a catalyst for the destruction of organic pollutants is the degree of mineralization. According to this parameter, the most effective

sample allowed achieving MB mineralization of 97 %, which is significantly higher than for Fe_2GeS_4 (56.3 %) and MgO_2/Fe^{3+} (70.2 %). The $CuCr_2O_4/CeO_2$ composite is characterized by a higher k' value and a lower time of MB catalytic degradation. However, data on the degree of mineralization for this sample were not provided, which did not allow us to make an entry about its effectiveness.

4 Conclusion

Magnesium ferrites doped with 10.0 mol. % of lanthanide ions (La^{3+}, Ce^{3+}, Sm^{3+}, Gd^{3+}, and Dy^{3+}) were successfully synthesized by the glycine-nitrate method. The regularities of changes in the parameters of the crystal structure depending on the conditions of synthesis of doped ferrites were established using XRD, FT-IR, SEM-EDX, and TEM techniques. It was shown that, depending on the dopant ion, magnesium ferrites with a crystal lattice parameter in the range of 8.387 – 8.431 Å and a unit cell volume of 0.590 – 0.599 nm^3 were obtained. Due to the inhibitory effect of lanthanide ions, the introduction of dopant ions into the magnesium ferrite composition makes it possible to obtain samples with an average crystallite size from 12.4 to 19.4 nm. The regularities of changes in the catalytic activity of heterogeneous Fenton catalysts under dark-, visible-, and UV-radiation were established. The positive effect of doping magnesium ferrite with lanthanide ions on the UV-driven photo-Fenton process was established and this was accompanied by the interaction of 3d-4f orbitals and the formation of impurity states in the band gap that increased ·OH radicals generation. An increase of calcination temperature from 300 to 600 °C led to dehydroxylation of magnesium ferrites and a dramatic decrease in their catalytic activity. The most active samples of magnesium ferrites provided a MB degradation degree of 95-99 % for 20 and 60 min for the Fenton and photo-Fenton processes. The catalysts reusability was confirmed during four catalytic cycles under visible light irradiation. The obtained heterogeneous catalyst performed enhanced catalytic activity in comparison with other high effective materials and applicable for wastewater treatment from dye pollutants.

CRediT (Contributor Roles Taxonomy) author statement

Andrei Ivanets: Conceptualization, Methodology, Writing-Original Draft, **Vladimir Prozorovich:** Investigation, Results discussion; **Marina Roshchina:** Magnesium ferrite samples synthesis; **Valentin Sarkisov:** Visualization, Data Curation; **Inga Grigoraviciute-Puroniene:** Editing, Formal analysis; **Aleksej Zarkov:** Editing; **Vhahangwele Masindi:** Editing, Formal analysis; **Chongqing Wang:** Editing, Formal analysis; **Aivaras Kareiva:** Editing, Formal analysis; **Varsha Srivastava:** Investigation, Editing; **Mika Sillanpää:** Project administration, Resources, Editing.

Declaration of Competing Interest

No conflict of interest.

Acknowledgements

This work was supported by travel grant of MOST Program for A. Ivanets (No. R-wY4k-52961) and V. Prozorovich (No. R-Jae2-52969).

References

[1] K.K. Kefeni, T.A.M. Msagati, Th.T.I. Nkambule, Bh.B. Mamba, Spinel ferrite nanoparticles and nanocomposites for biomedical applications and their toxicity. Mater. Sci. Eng., C. 107 (2020) 110314. https://doi.org/10.1016/j.msec.2019.110314.

[2] M. Amiri, M. Salavati-Niasari, Ah. Akbari, Magnetic nanocarriers: Evolution of spinel ferrites for medical applications. Adv. Colloid Interface Sci. 265 (2019) 29-44. https://doi.org/10.1016/j.cis.2019.01.003.

[3] D.H.K. Reddy, Y.-S. Yun, Spinel ferrite magnetic adsorbents: Alternative future materials for water purification? Coord. Chem. Rev. 315 (2016) 90-111. https://doi.org/10.1016/j.ccr.2016.01.012.

[4] K.K. Kefeni, Bh.B. Mamba, T.A.M. Msagati, Application of spinel ferrite nanoparticles in water and wastewater treatment: A review. Sep. Purif. Technol. 188 (2017) 399-422. https://doi.org/10.1016/j.seppur.2017.07.015.

[5] Ch.M. Park, Y.M. Kim, K.-H. Kim, D. Wang, Ch. Su, Y. Yoon, Potential utility of graphene-based nano spinel ferrites as adsorbent and photocatalyst for removing organic/inorganic contaminants from aqueous solutions: A mini review. Chemosphere. 221 (2019) 392-402. https://doi.org/10.1016/j.chemosphere.2019.01.063.

[6] N. Thomas, D.D. Dionysiou, S.C. Pillai, Heterogeneous Fenton catalysts: A review of recent advances. J. Hazard. Mater. 404 (B) (2021) 124082. https://doi.org/10.1016/j.jhazmat.2020.124082.

[7] K.K. Kefeni, Bh.B. Mamba, Photocatalytic application of spinel ferrite nanoparticles and nanocomposites in wastewater treatment: Review. Sustainable Mater. Technol. 23 (2020) e00140. https://doi.org/10.1016/j.susmat.2019.e00140.

[8] M. Amiri, Kh. Eskandari, M. Salavati-Niasari, Magnetically retrievable ferrite nanoparticles in the catalysis application. Adv. Colloid Interface Sci. 271 (2019) 101982. https://doi.org/10.1016/j.cis.2019.07.003.

[9] T. Tatarchuk, M. Bououdina, J.J. Vijaya, L.J. Kennedy, Spinel Ferrite Nanoparticles: Synthesis, Crystal Structure, Properties, and Perspective Applications. In: Fesenko, O., Yatsenko, L. (Eds.), Nanophysics, Nanomaterials, Interface Studies, and Applications. NANO 2016. Springer Proceedings in Physics. 195 (2017), pp. 305-325. https://doi.org/10.1007/978-3-319-56422-7_22.

[10] S.B. Narang, K. Pubby, Nickel Spinel Ferrites: A review. J. Magn. Magn. Mater. 519 (2021) 167163. https://doi.org/10.1016/j.jmmm.2020.167163.

[11] G. Dhillon, N. Kumar, M. Chitkara, I.S. Sandhu, Effect of A-site substitution and calcination temperature in Fe_3O_4 spinel ferrites. J. Mater. Sci.: Mater. Electron. 31 (21) (2020) 18903-18912. https://doi.org/10.1007/s10854-020-04427-y.

[12] C. Murugesan, K. Ugendar, L. Okrasa, J. Shen, G. Chandrasekaran, Zinc substitution effect on the structural, spectroscopic and electrical properties of nanocrystalline $MnFe_2O_4$ spinel ferrite. Ceram. Int. 47 (2) (2021) 1672-1685. https://doi.org/10.1016/j.ceramint.2020.08.284.

[13] N.N. Sarkar, S.A. Tirpude, P.S. Sawadh, K.G. Rewatkar, Effect of cobalt and nickel substitution on structural and magnetic properties of spinel ferrite. Integr. Ferroelectr. 203 (1) (2019) 61-66. https://doi.org/10.1080/10584587.2019.1674966.

[14] H.St.C. O'Neill, H. Annersten, D. Virgo, The temperature dependence of the cation distribution in magnesioferrite ($MgFe_2O_4$) from powder XRD structural refinements and Mossbauer spectroscopy. Am. Mineral. 77 (7-8) (1992) 725-740.

[15] L.T.T. Nguyen, N.C. Manh, D.N. Quoc, H.N. Quang, H.T.T. Nguyen, D.Ch. Nguyen, L.G. Bach, A facile synthesis, characterization, and photocatalytic activity of magnesium ferrite nanoparticles via the solution combustion method. J. Chem. 2019 (2019) 3428681. https://doi.org/10.1155/2019/3428681.

[16] S. Thankachan, M. Kurian, D.S. Nair, Sh. Xavier, E.M. Mohammed, Effect of rare earth doping on structural, magnetic, electrical properties of magnesium ferrite and its catalytic activity. Int. J. Eng. Sci. Innovative Technol. 3 (4) (2014) 529-537.

[17] R. Kant, A.K. Mann, A review of doped magnesium ferrite nanoparticles: introduction, synthesis, techniques and applications. Int. J. Sci. Res. Sci. Eng. Technol. 4 (7) (2018) 646-660. https://doi.org/10.32628/IJSRSET1848216.

[18] M. Dhiman, B. Chudasama, V. Kumar, K.B. Tikoo, S. Singhal, Augmenting the photocatalytic performance of cobalt ferrite via change in structural and optical properties with the introduction of different rare earth metal ions. Ceram. Int. 45 (3) (2019) 3698-3709. https://doi.org/10.1016/j.ceramint.2018.11.033.

[19] P. Samoila, C. Cojocaru, L. Sacarescu, P.P. Dorneanu, A.-A. Domocos, A. Rotaru, Remarkable catalytic properties of rare-earth doped nickel ferrites synthesized by sol-gel auto-combustion with maleic acid as fuel for CWPO of dyes. Appl. Catal., B. 202 (2017) 21-32. https://doi.org/10.1016/j.apcatb.2016.09.012.

[20] A. Rahman, M.F. Warsi, I. Shakir, M. Shahid, S. Zulfiqar, Fabrication of Ce^{3+} substituted nickel ferrite-reduced graphene oxide heterojunction with high photocatalytic activity under visible light irradiation. J. Hazard. Mater. 394 (2020) 122593. https://doi.org/10.1016/j.jhazmat.2020.122593.

[21] D. Hermosilla, C. Han, M.N. Nadagouda, L. Machala, A. Gascó, P. Campo, D.D. Dionysiou, Environmentally friendly synthesized and magnetically recoverable designed ferrite photo-catalysts for wastewater treatment applications. J. Hazard. Mater. 381 (2020) 121200. https://doi.org/10.1016/j.jhazmat.2019.121200.

[22] A. Ivanets, V. Prozorovich, M. Roshchina, T. Kouznetsova, N. Budeiko, L. Kulbitskaya, A. Hosseini-Bandegharaei, Vh. Masindi, V. Pankov, A comparative study on the synthesis of magnesium ferrite for the adsorption of metal ions: Insights into the essential role of crystallite size and surface hydroxyl groups. Chem. Eng. J. 411 (2021) 128523. https://doi.org/10.1016/j.cej.2021.128523.

[23] A. Ivanets, M. Roshchina, V. Srivastava, V. Prozorovich, T. Dontsova, S. Nahirniak, V. Pankov, A. Hosseini-Bandegharaei, H.N. Tran, M. Sillanpää, Effect of metal ions

adsorption on the efficiency of methylene blue degradation onto $MgFe_2O_4$ as Fenton-like catalysts. Colloids Surf., A. 571 (2019) 17-26. https://doi.org/10.1016/j.colsurfa.2019.03.071.

[24] A.I. Ivanets, V. Srivastava, M.Yu. Roshchina, M. Sillanpää, V.G. Prozorovich, V.V. Pankov, Magnesium ferrite nanoparticles as a magnetic sorbent for the removal of Mn^{2+}, Co^{2+}, Ni^{2+} and Cu^{2+} from aqueous solution. Ceram. Int. 44 (8) (2018) 9097-9104. https://doi.org/10.1016/j.ceramint.2018.02.117.

[25] K.V. Kumar, K. Porkodi, A. Selvaganapathi, Constrain in solving Langmuir–Hinshelwood kinetic expression for the photocatalytic degradation of Auramine O aqueous solutions by ZnO catalyst. Dyes Pigm. 75 (1) (2007) 246-249. https://doi.org/10.1016/j.dyepig.2006.05.035.

[26] Y. Liu, Y. Zhao, J. Wang, Fenton/Fenton-like processes with in-situ production of hydrogen peroxide/hydroxyl radical for degradation of emerging contaminants: Advances and prospects. J. Hazard. Mater. 404 (B) (2021) 124191. https://doi.org/10.1016/j.jhazmat.2020.124191.

[27] Y. Wang, H. Zhao, M. Li, J. Fan, G. Zhao, Magnetic ordered mesoporous copper ferrite as a heterogeneous Fenton catalyst for the degradation of imidacloprid. Appl. Catal., B. 147 (2014) 534-545. https://doi.org/10.1016/j.apcatb.2013.09.017.

[28] Gh.A. Ashraf, R.T. Rasool, M. Hassan, L. Zhang, H. Guo, Heterogeneous catalytic activation of BaCu-based M-hexaferrite nanoparticles for methylene blue degradation under photo-Fenton-like system. Mol. Catal. 505 (2021) 111501. https://doi.org/10.1016/j.mcat.2021.111501.

[29] X. Wang, D. Li, Zh. Nan, Effect of N content in g-C_3N_4 as metal-free catalyst on H_2O_2 decomposition for MB degradation. Sep. Purif. Technol. 224 (2019) 152-162. https://doi.org/10.1016/j.seppur.2019.04.088.

[30] X. Shi, A. Tian, J. You, H. Yang, Y. Wang, X. Xue, Degradation of organic dyes by a new heterogeneous Fenton reagent – Fe_2GeS_4 nanoparticle. J. Hazard. Mater. 353 (2018) 182-189. https://doi.org/10.1016/j.jhazmat.2018.04.018.

[31] D. Wu, Y. Bai, W. Wang, H. Xia, F. Tan, Sh. Zhang, B. Su, X. Wang, X. Qiao, P.K. Wong, Highly pure MgO_2 nanoparticles as robust solid oxidant for enhanced Fenton-like degradation of organic contaminants. J. Hazard. Mater. 374 (2019) 319-328. https://doi.org/10.1016/j.jhazmat.2019.04.058.

[32] K. Ghorai, A. Panda, M. Bhattacharjee, D. Mandal, A. Hossain, P. Bera, Md. Motin Seikh, A. Gayen, Facile synthesis of $CuCr_2O_4/CeO_2$ nanocomposite: A new Fenton like catalyst with domestic LED light assisted improved photocatalytic activity for the degradation of RhB, MB and MO dyes. Appl. Surf. Sci. 536 (2021) 147604. https://doi.org/10.1016/j.apsusc.2020.147604.

[33] D. Li, T. Yang, Y. Li, Zh. Liu, W. Jiao, Facile and green synthesis of highly dispersed tar-based heterogeneous Fenton catalytic nanoparticles for the degradation of methylene blue. J. Cleaner Prod. 246 (2020) 119033, https://doi.org/10.1016/j.jclepro.2019.119033.

[34] X. Huang, L. Liu, Z. Xi, H. Zheng, W. Dong, G. Wang, One-pot solvothermal synthesis of magnetically separable rGO/$MnFe_2O_4$ hybrids as efficient photocatalysts for degradation of MB under visible light. Mater. Chem. Phys. 231 (2019) 68-74. https://doi.org/10.1016/j.matchemphys.2019.03.076.